

# Kinetics of Trifurcated Electron Flow in the Deca-heme Bacterial Proteins MtrC and MtrF

Xiuyun Jiang<sup>a</sup>, Bastian Burger<sup>a,b</sup>, Fruzsina Gajdos<sup>a</sup>, C. Bortolotti<sup>c</sup>, Zdenek Futera<sup>a</sup>, Marian Breuer<sup>a</sup>, and Jochen Blumberger<sup>a,d,1</sup>

<sup>a</sup>University College London, Department of Physics and Astronomy, Gower Street, London WC1E 6BT, UK; <sup>b</sup>Technische Universität München, Department of Chemistry, Lichtenbergstrasse 4, D-85747 Garching, Germany; <sup>c</sup>Università degli Studi di Modena e Reggio Emilia, Department of Life Sciences, Via Università 4, 41121 Modena, Italy; <sup>d</sup>Institute for Advanced Study, Technische Universität München, Lichtenbergstrasse 2 a, D-85748 Garching, Germany

This manuscript was compiled on January 7, 2019

1 **The bacterium *Shewanella oneidensis* has evolved a sophisticated**  
2 **electron transfer machinery to export electrons from the cytosol**  
3 **to extracellular space during extracellular respiration. At the heart**  
4 **of this process are deca-heme proteins of the Mtr pathway, MtrC**  
5 **and MtrF, located at the external face of the outer bacterial mem-**  
6 **brane. Crystal structures have revealed these proteins bind 10 c-**  
7 **type hemes arranged in the peculiar shape of a staggered cross**  
8 **that trifurcates the electron flow, presumably to reduce extracellu-**  
9 **lar substrates while directing electrons to neighbouring MHCs at ei-**  
10 **ther sides along the membrane. Especially intriguing is the design**  
11 **of the heme junctions trifurcating the electron flow: they are made**  
12 **of co-planar and T-shaped heme pair motifs with relatively large and**  
13 **seemingly unfavourable tunneling distances. Here we use electronic**  
14 **structure calculations and molecular simulation to show that the side**  
15 **chains of the heme rings, in particular the cysteine linkages inserting**  
16 **in the space between co-planar and T-shaped heme pairs, strongly**  
17 **enhance electronic coupling in these two motifs. This results in a**  
18  **$\approx 10^3$ -fold speed-up of ET steps at heme junctions that would other-**  
19 **wise be rate-limiting. The predicted maximum electron flux through**  
20 **the solvated proteins is remarkably similar for all possible flow direc-**  
21 **tions, suggesting that MtrC and MtrF shuttle electrons with similar**  
22 **efficiency and reversibly in directions parallel and orthogonal to the**  
23 **outer membrane. No major differences in the ET properties of MtrC**  
24 **and MtrF are found implying that the different expression levels of**  
25 **the two proteins during extracellular respiration is not related to re-**  
26 **dox function.**

extracellular respiration | electron transfer | heme | molecular dynamics  
| density functional theory

1 **M**ulti-heme cytochromes (MHC) are expressed by the  
2 bacteria *Shewanella oneidensis* and *Geobacter sulfurre-*  
3 *ducens* to shuttle electrons from the inside of the cell across  
4 the periplasm and outer membrane to extracellular space in  
5 a process termed extracellular respiration(1). They are part  
6 of a fascinating electron export machinery that allows the  
7 bacterium to survive at reduced O<sub>2</sub> levels by transferring elec-  
8 trons, accumulated by metabolic activity, to electron acceptors  
9 *outside* the cell, e.g. transition metal oxide minerals Fe<sub>2</sub>O<sub>3</sub>  
10 and MnO<sub>2</sub>. The bacteria's ability to electronically wire the  
11 cytosol with extracellular space has attracted much interest  
12 for their use in the clean-up of water and soil containing ra-  
13 dioactive isotopes(2), for mediatorless microbial fuel cells(3, 4)  
14 and microbial electrosynthesis(5–7) (see review Ref. (8)). The  
15 exquisite electron transfer properties of their MHCs has also  
16 sparked much interest for their use in bioelectronic junctions  
17 and devices(9–12). It was recently shown that two MHCs  
18 from *S. oneidensis*, STC and MtrF, are up to 1000-fold more  
19 conductive than other metallo-proteins such as azurin and

single-heme cytochromes(12), which might open up a host of  
new electronic applications at the biotic/abiotic interface.

Crystal structures of several MHCs have been resolved in  
recent years(13–17); the structures of some of the most promi-  
nent MHCs of *S. oneidensis* are shown in fig. 1. Among the  
largest, the deca-heme proteins MtrC(17) and MtrF(15) (pan-  
els A and B) arrange ten tightly packed bis-His coordinated  
c-type hemes in the peculiar shape of a staggered cross: a  
vertically aligned octa-heme chain is intersected horizontally  
by a tetra-heme chain. Located on the external surface of  
the outer membrane, MtrC (MtrF) is part of the MtrCAB  
(MtrFDE) complex that spans the outer membrane (see panel  
E) and transmits electrons over distances larger than 100 Å.  
Electron input from the electron donor MtrA (MtrD) occurs  
at one of the termini of the octa-heme chain, speculated to  
be heme 10(15). Subsequent electron flow through MtrC may  
occur in three different directions, along the octa-heme chain  
to heme 5, or towards the side exits of the tetra-heme chain,  
hemes 2 and 7.

While there may be multiple reasons for the evolution of  
cytochromes that feature a staggered heme cross, a clue for  
a possible functional role came from recent in-vivo(18) and  
electron cryotomography studies(19). It was shown that the  
micrometer-long cellular appendages that *S. oneidensis* form  
upon reduced O<sub>2</sub> levels (sometimes referred to as “biologi-  
cal nanowires”) are in fact extensions of the outer membrane  
rather than pilin-based structures(20, 21), with MtrCAB dis-

## Significance Statement

Certain bacteria survive in anoxic environments by switching from aerobic to anaerobic respiration: in place of O<sub>2</sub> they reduce diverse substrates *outside* the cell. Multi-heme cytochromes (MHC) spanning the outer membrane have been identified as the essential building blocks for this process. Here we provide molecular-level insight into the electron flow in two deca-heme proteins. Our study reveals that electron hopping through these proteins is strongly enhanced by cysteines at heme junctions that trifurcate the electron flow. We believe this to be a general design principle in MHCs for acceleration of ET steps that would otherwise be too slow for respiration. Our study uncovers a natural design principle of significance to an entire class of proteins involved in biological ET.

X.J., B.B., F.G. and C.B. carried out molecular simulations, Z.F. contributed computer code, X.J., M. B. and J.B. analyzed results and J.B. designed the work.

The authors declare no conflict of interest.

<sup>1</sup>To whom correspondence should be addressed. E-mail: j.blumberger@ucl.ac.uk (J.B.)

tributed along their length(18, 19), as schematically indicated in fig. 1E. Adjacent MtrCAB complexes are thought to interact via the tetra-heme chains of MtrC to facilitate micro-meter long electron transfer along the outer membrane as observed by c-AFM(22), while the octaheme-chains support ET away from the membrane and on to extracellular substrates. In this way, the heme cross motif helps supply the surface of the membrane with electrons while reducing extracellular substrates. Yet, the kinetics of the trifurcated electron flow in MtrC remains to be elucidated; does this protein transfer electrons equally well in the direction parallel to the membrane and away from it?

In our previous work we have used quantum chemistry and molecular simulation to obtain a first insight into the workings of solvated MHCs at the single-protein level.(23–25) In an early study, we calculated the reduction potentials for all 10 hemes in all-oxidized (all-ox) MtrF using MD simulation(26), and more recently Barrozo *et al.* reported heme reduction potentials for MtrF and MtrC in the all-ox and all-reduced (all-red) states(27). Both studies agreed that the free energy profile for electron flow along the protein has ups and downs, yet resulting in near thermoneutral ET along the octaheme chain. In terms of kinetics, we found that heme-heme electronic couplings are about three orders of magnitude smaller than reorganization free energy, which implies that intraprotein ET through solvated MHCs occurs via heme-to-heme hopping. However, our calculations fell short of reproducing the  $\approx$  nano-Ampere (nA) currents reported in STM measurements(9, 11). Even after accounting for partial protein hydration in these experiments, the computed STM currents remained underestimated by about two orders of magnitude.

This discrepancy has motivated us to take a closer look at the staggered cross heme motif built into MtrC and MtrF. The trifurcation of the electron flow is established by two junctions in the middle of the protein comprised of T-shaped (8-6, 1-3) and co-planar heme pairs (6-1, 6-7, 1-2). Inspection of the crystal structure reveals relatively large heme-to-heme edge distances in these motifs suggesting that the ET steps across the junctions may limit to overall electron flow through the protein. In this respect, we note that the smaller tetra-heme protein STC (fig. 1 (D)) also features two T-shaped heme pairs, similarly as in MtrF and MtrC, though no co-planar pairs. We found that cysteine linkages, which chemically attach the heme rings to the protein frame, enhance electronic coupling between the T-shaped heme pairs in STC. The effect of the cysteine linkages has not been included in our previous computations on MtrF(28) and calls for a re-calculation of electronic couplings for this protein, especially in the context of the persisting mismatch between computation and experiment for STM currents(11).

Returning to the bacterium *S. oneidensis*, a puzzling observation is that under anoxic conditions only MtrCAB and no MtrDEF is expressed, even though it is known that MtrF can functionally replace MtrC(29, 30). As pointed out by Barrozo *et al.*(27), this apparent redundancy is unusual and the conditions under which the genes for MtrDEF are expressed remain largely unknown. It begs the question whether different expression levels of the two proteins is due to differences in their electron transfer properties. Does MtrC conduct electrons better than MtrF? To answer this and the above questions we present in the current paper all ET parameters, heme-to-heme

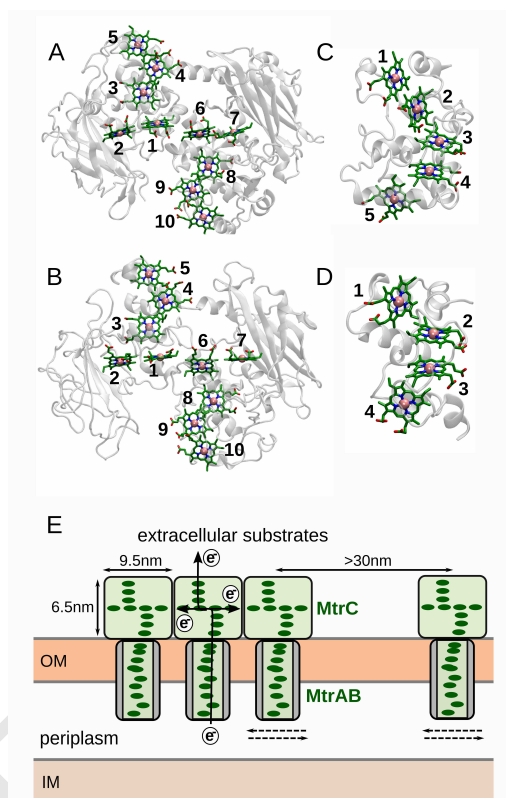


**Fig. 1.** Crystal structures of decaheme cytochromes MtrC, pdb id: 4LM8(17) (A); MtrF, pdb id: 3PMQ(15) (B); penta-heme cytochrome NrfB, pdb id: 2OZY(13) (C) and tetraheme cytochrome STC, pdb id: 1M1Q(31) (D). The bis-His coordinated c-type heme rings are depicted in green, Fe atoms in purple and the protein secondary structures in grey. (E) Cartoon representation of a possible arrangement of MtrCAB complexes in the bacterial outer membrane during extracellular respiration (OM), inspired by the cryotomography study of Ref. (19). Electrons from the periplasm are transferred across the OM via the deca-heme protein complex MtrAB and passed on to the deca-heme protein MtrC where the electron flow is trifurcated in directions parallel and orthogonal to the OM. The spacing between the centers of adjacent MtrC and MtrA molecules is typically about 10 nm, i.e. close contact, but gaps larger than 30 nm were also observed and may be overcome by lateral protein diffusion within the membrane, as indicated by dashed arrows.(19) IM stands for inner bacterial membrane.

ET rate constants and protein-limited electron flux through MtrC, calculated for exactly the same conditions as for MtrF. This undertaking is very timely because the crystal structure of MtrC has recently become available. Whilst Barrozo *et al* have recently presented a preliminary characterization of the ET kinetics for MtrC,(27) though with outdated electronic couplings from MtrF, a full and up-to-date characterization for this protein is outstanding.

## Results

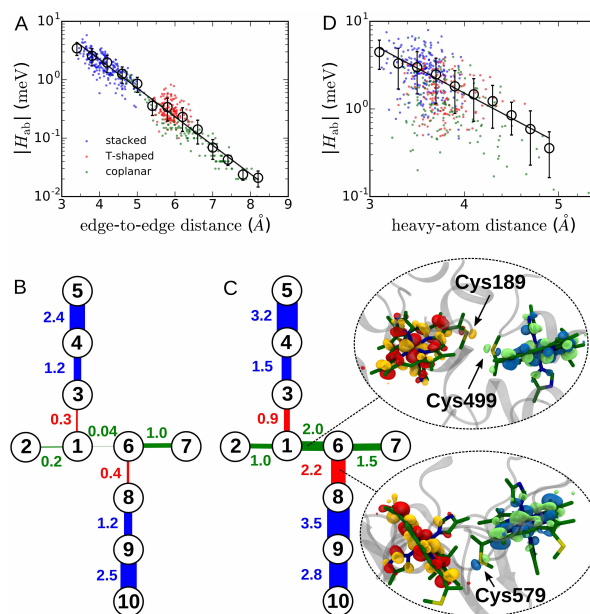
**Heme-heme electronic interaction.** Electronic coupling matrix elements for electron hopping between adjacent  $\text{Fe}^{2+}/\text{Fe}^{3+}$ -heme pairs have been calculated along molecular dynamics trajectories for the solvated MtrC and MtrF. The coupling calculations were carried out for two QM models on structures extracted from the MD run, one where the two bis-His hemes are modelled by unsubstituted Fe-porphin rings axially ligated by two N-methyl imidazoles, hereafter referred to as the mini-

125 mum model, and one where, in addition, all of the side chains  
 126 of both heme rings are included, hereafter referred to as the  
 127 large model. Details on the MD simulations and the density  
 128 functional theory (DFT)-based coupling calculations can be  
 129 found in *Materials and Methods* and in the SI appendix.

130 The results are shown in fig. 2, where we have also included  
 131 previously reported couplings for the small tetra-heme protein  
 132 STC(32). The data for the minimum model (panel A) show the  
 133 expected exponential decay with respect to the heme edge-to-  
 134 heme edge distance  $r$ ,  $\langle |H_{ab}|^2 \rangle^{1/2} = A \exp[-\beta(r-r_0)/2]$ . The  
 135 scatter around the mean values is due to thermal motion of the  
 136 heme rings ( $T=300$  K). The couplings decrease in the order  
 137 stacked > T-shaped > co-planar heme-heme motif. In the  
 138 stacked motif the hemes approach one another up to van-der-  
 139 Waals distance (3.5–5 Å) resulting in couplings of several meVs,  
 140 whereas in the T-shaped and co-planar motifs the edge-to-edge  
 141 distances are larger (5–8 Å), and the couplings are an order  
 142 of magnitude smaller, typically a few 0.1 meV or less. The  
 143 distance decay constant  $\beta$  and the prefactor  $A$  are determined  
 144 to be 2.26 Å<sup>-1</sup> and 3.49 meV, respectively ( $R^2 = 0.99$ ,  $r_0 =$   
 145 3.6 Å), in good agreement with the ones reported previously for  
 146 data from MtrF only(28). The thermally averaged couplings  
 147 for each heme pair of MtrC are depicted in fig. 2B clearly  
 148 illustrating how the couplings decrease from relatively large  
 149 values for the stacked motif at electron input and exit sites  
 150 of the octa-heme chain (hemes 10 and 5), to smaller values  
 151 for the T-shaped and co-planar motifs in the middle of the  
 152 protein. Particularly small is the electronic coupling for the  
 153 co-planar pair 1-6 in the center of the protein due to their  
 154 relatively large edge-to-edge distance (7.0 Å in the crystal  
 155 structure(17)).

156 Yet, the situation is strikingly different when the heme  
 157 side chains are included in the coupling calculation. While  
 158 the values for the stacked motif hardly change, they increase  
 159 significantly for co-planar and T-shaped motifs, respectively,  
 160 to values that are just slightly below the ones for the stacked motif  
 161 (fig. 2C). Consequently, all couplings now fall in a rather narrow  
 162 range of about 0.9-3.5 meV for MtrC (0.7-4.5 meV for MtrF).  
 163 For further discussion, we define the coupling enhancement  
 164 as the ratio  $r_{\text{dft}}^{1/2} = [(\langle |H_{ab}^1|^2 \rangle) / (\langle |H_{ab}^m|^2 \rangle)]^{1/2}$ , where  $H_{ab}^1$  and  $H_{ab}^m$   
 165 are the coupling matrix element for heme-to-heme electron  
 166 tunneling for the large (l) and minimum (m) QM models, and  
 167  $\langle \dots \rangle$  denotes the thermal average over MD snapshots. We  
 168 find that most of the coupling enhancement is due to the  
 169 cysteine linkages that insert in the space between co-planar  
 170 and T-shaped heme motifs (inset of panel C). In case of the  
 171 co-planar heme pair 1-6, where the coupling enhancement  
 172 effect is the greatest ( $r_{\text{dft}}^{1/2} = 50$  for MtrC (30 for MtrF)),  
 173 Cys189(197) and Cys499(476) which covalently link hemes 1  
 174 and 6 to the protein backbone, approach one another up to  
 175 a S-S distance of 4.0 (3.8) Å. According to our calculations,  
 176 the sulfur 3p orbital of Cys189(197) weakly mixes with the Fe-  
 177 heme frontier orbitals of heme 1, and a similar mixing occurs  
 178 for Cys499(476) and heme 6. The small delocalization of the  
 179 frontier orbital over the S atoms leads to a sizable increase in  
 180 orbital overlap and consequently electronic coupling. Similar  
 181 albeit smaller coupling enhancements occur for the T-shaped  
 182 pairs 8-6 ( $r_{\text{dft}}^{1/2} = 6$  (8)) and 1-3 ( $r_{\text{dft}}^{1/2} = 3$  (4)), where only one  
 183 cysteine inserts between the hemes.

184 A consequence of the mixing of frontier orbital amplitude  
 185 over heme side chains is that the heme edge-to-heme edge



186 **Fig. 2.** Heme-heme electronic coupling matrix elements,  $|H_{ab}|$ , in MtrC, MtrF and  
 187 STC. The distance dependence of electronic couplings is shown in (A) for the minimum  
 188 (m) QM model ( $H_{ab} = H_{ab}^m$ ) comprised of the unsubstituted heme rings plus axial  
 189 ligands and in (D) for the large (l) QM model ( $H_{ab} = H_{ab}^l$ ) where, in addition, all  
 190 heme side chains are included, in particular the Cys linkages. The couplings are  
 191 calculated on structures obtained from MD simulation at room temperature. They are  
 192 color-coded according to the relative orientations of electron donating and accepting  
 193 hemes: stacked motif in blue (heme pairs 10-9, 9-8, 3-4, 4-5 in MtrC and MtrF and  
 194 2-3 in STC), T-shaped in red (8-6 and 1-3 in MtrC and MtrF and 1-2, 3-4 in STC), and  
 195 co-planar in green (6-1, 6-7 and 1-2 in MtrC and MtrF). Root-mean-square averages  
 196 of the scattered data points were calculated for bins of width 0.4 Å (A) and 0.2 Å (D)  
 197 and are denoted by black circles with error bars indicating the root-mean-square  
 198 fluctuations. Fits to an exponential are indicated by a black line. In (A) the shortest  
 199 heme edge-to-edge distance is used and in (B) the shortest distance between any  
 200 heavy atom of heme ring and side chains. Electronic couplings averaged for each  
 201 adjacent heme pair in MtrC,  $\langle |H_{ab}|^2 \rangle^{1/2}$ , are indicated for the minimum QM model  
 202 (panel B) and for the large QM model (panel C). The thickness of the bars connecting  
 203 adjacent hemes is proportional to the average coupling. The insets in (C) depict  
 204 the enhancement of electronic couplings due to Cys linkages inserting in the space  
 between co-planar heme pair 6-1, and T-shaped heme pair 8-6. One of the three Fe  
 $d(t_{2g})$ -heme orbitals on electron donor and acceptor hemes contributing to electronic  
 coupling are drawn as red/yellow and green/blue isosurfaces (denoted  $d_i^d$  and  $d_j^a$  in  
 SI appendix). Similar coupling enhancements are found for MtrF.

186 distance is no longer a good distance metric for heme-to-heme  
 187 electron tunneling. The spread of coupling values around the  
 188 best fit for exponential distance decay is very large ( $R^2 = 0.57$ ,  
 189 see SI Appendix, fig. S1). Instead, we use the shortest distance  
 190 between any heavy atom (C, N, O, S) of the porphyrin ring plus  
 191 side chains. Using this metric, all couplings shift to shorter  
 192 distances and can be fit to an exponential distance decay with  
 193 parameters similar to the ones for the minimum model in  
 194 panel (A),  $\beta = 2.63$  Å<sup>-1</sup>,  $A = 2.57$  meV ( $R^2 = 0.97$ , fig. 2D),  
 195 characteristic for through-space tunneling. Yet, the scatter  
 196 around the mean values is still significantly larger than for  
 197 the minimum model. Most likely, this is because the degree of  
 198 delocalization of the frontier orbitals over the side chains varies  
 199 more strongly with intramolecular heme geometry than for the  
 200 unsubstituted porphyrine rings and this effect is independent  
 201 on inter-heme distance.

202 We would like to emphasize that electronic couplings calcu-  
 203 lated here are for through-space tunneling between adjacent  
 204 heme cofactors including all side chains and the Cys link-



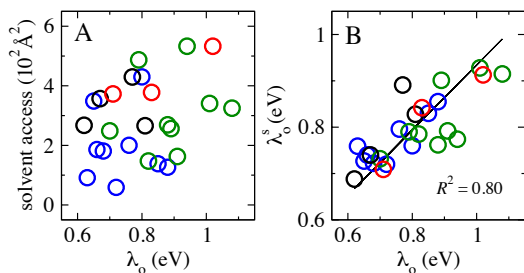


**Fig. 3.** Outer-sphere reorganization free energy,  $\lambda_0$ , for heme-to-heme ET in MtrC (blue), MtrF (green), NrFb (black) and STC (red), as obtained from MD simulations. Values for MtrC and NrFb taken from current simulations (SI Appendix, Table S1), values for MtrF taken from Ref. (35) and for STC from Ref. (32). Correlations are shown between  $\lambda_0$  and (A) the solvent accessible surface area (SA)(36) of corresponding heme pairs, (B) Marcus continuum estimates for outer-sphere reorganization free energy,  $\lambda_0^s$  with SA-dependent static dielectric constant (see main text for details).

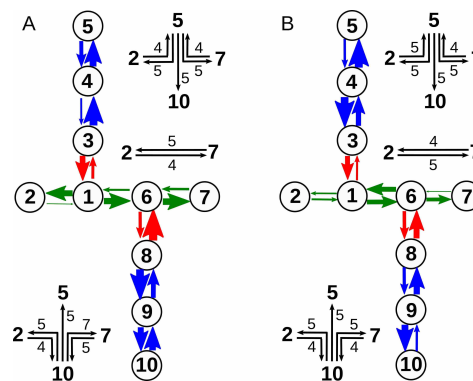


**Fig. 4.** Kinetics of trifurcated electron flow in solvated MtrC (A) and MtrF (B). The thickness of the colored arrows connecting hemes is proportional to the heme-to-heme ET rate constants in the all-ox state, summarized in SI Appendix, Table S1. See Fig. 1 for heme numbering. Insets show the possible flow directions between the terminal hemes 10, 5, 7, 2 with the logarithm of the maximum, protein-limited steady-state electron flux,  $\log_{10}(J_{\max}/s^{-1})$ , indicated for each flow direction. The electron flux is obtained by solving a chemical Master equation, see *Materials and Methods* and SI for details.  $J_{\max}$  is taken from SI Appendix, Table S2 (“ox-sc<sup>a</sup>”).

ages of the heme groups. Hence, the  $\beta$  values reported here are about a factor of two larger than the typical range for through-protein tunneling, 1.0-1.5  $\text{\AA}^{-1}$ (25), whilst the tunneling distance for each consecutive hop is about a factor of 2 or more smaller than for typical through-protein tunneling processes. As is well known, over distances of several nanometers and beyond multi-step hopping outcompetes 1-step tunneling due to its favourable  $1/R$  scaling compared with exponential scaling for 1-step tunneling.(25) There are amino acid side chains that bridge the gap between co-planar and T-shaped heme pairs (e.g. between hemes 1 and 6, ILE252, LEU571 in MtrC and PRO540, PRO243 in MtrF), implying that amino acid-mediated heme-to-heme tunneling could be an alternative mechanism. However, using pathway calculations(33, 34), we found that the dominant through-space tunneling path always gave couplings at least an order of magnitude higher than any amino acid-mediated pathway, which rules out this alternative mechanism, at least at the level of pathway calculations.

**Reorganization free energy and driving force.** We have calculated the reorganization free energy  $\lambda$  for ET between all adjacent hemes in MtrC using MD simulations. For the purpose of deriving fit parameters for  $\lambda$  in MHCs, we also computed  $\lambda$  for the penta-heme MHC NrFb and take values for MtrF(35) and STC(32) from our previous work. We find that the values for all four proteins fall in the range 0.7-1.1 eV with values for MtrC being slightly smaller on average than for MtrF (see Table S1). Interestingly, the dominating outer-sphere reorganization free energy due to protein and solvent,  $\lambda_0$ , does not correlate with the solvent accessible surface area (SA) of the heme pairs (fig. 3A), but can be well described by Marcus’ continuum formula if the static dielectric constant is assumed to be a linear function of the SA,  $\epsilon_s(SA) = a + bSA$ ,  $a, b$  constants. The smallest mean deviation with respect to  $\lambda_0$  from MD is obtained for  $a = 5.18$ ,  $b = 0.016 \text{\AA}^{-2}$  and an effective heme radius  $r = 4.6 \text{\AA}$ (using an optical dielectric constant,  $\epsilon_{op} = 1.84$ (37)), see fig. 3B. This gives  $\epsilon_s$  values between 6 (for the buried heme pair 1-3 of MtrC) and 14 (for the strongly solvent exposed heme pair 10-9 of MtrF).

ET driving forces are calculated for the all-ox redox state of MtrC using molecular dynamics combined with thermodynamic integration. The resultant free energy profile for ET along the heme chains (Table S1) is qualitatively similar to the one reported recently by Barrozo *et al.* for the same redox

state, denoted “Electron hopping regime” in their work(27), and is not further discussed here. For MtrF, ET driving forces are taken from our previous work(26).

**Electron flux through MtrC and MtrF.** The computed electronic couplings, reorganization free energies and driving forces are used to calculate the non-adiabatic (Marcus) rate constants for all heme-to-heme ET steps. They are used as an input for a chemical Master equation for electron hopping, which we solve to obtain the maximum, protein-limited electron flux through MtrC and MtrF. Briefly, we assume fast and irreversible electron input in a given terminal heme site, e.g. heme 10, and electron output from another terminal heme site, e.g. heme 5. The electron population of each single heme, which can take values between 0 (fully oxidized) and 1 (fully reduced), is determined subject to the condition of steady-state electron flux through the protein. Similar flux calculations are carried out for the reverse direction along the octa-heme chain and for ET from heme 10 and heme 5 to the side exits heme 7 and 2, respectively. Further details on the calculations can be found in the SI Appendix.

The results are illustrated in fig. 4 for MtrC (panel A) and MtrF (panel B). The heme-to-heme rate constants are proportional to the width of the arrows connecting hemes and the protein-limited electron flux for all 12 possible flow directions across MtrC and MtrF are shown in the insets (in powers of  $10 \text{ s}^{-1}$ ). The rate constants along the octa-heme chains of MtrC and MtrF span four orders of magnitude, from  $\approx 10^5 - 10^9 \text{ s}^{-1}$ , and the electron flux is  $\approx 10^5 \text{ s}^{-1}$  in both the  $10 \rightarrow 5$  and  $10 \leftarrow 5$  directions. Electron flow from hemes 10 or 5 to the side exits 7 and 2 is similarly fast as along the octa-heme main chain, about  $10^5 \text{ s}^{-1}$ , except for  $10 \rightarrow 7$  due to the relatively high reduction potential of heme 7. But the latter is subject to uncertainty as discussed previously(26, 27) and may be overestimated. The reverse flow from the side exits 7 or 2 to 10 and 5 is somewhat slower, typically about  $10^4 \text{ s}^{-1}$ , due to successive up-hill steps involving co-planar and T-shaped motifs. Similar results are obtained when the sets of reduction potentials from Barrozo *et al.* are used(27), with deviations of typically less than an order of magnitude (see

287 SI Appendix, Table S2). Overall, our results indicate that  
288 MtrC and MtrF conduct electrons about equally well along  
289 their main axis and in perpendicular directions with little or  
290 no directional bias.

291 Whilst the electron flux (with all heme side chains included)  
292 is remarkably similar for all directions, the electron flux en-  
293 hancement due to the side chains is not the same in every  
294 direction - on the contrary, depending on the number of co-  
295 planar and T-shaped heme pairs and their free energies for  
296 a given flow direction, the flux enhancement varies from be-  
297 tween a factor of 2 ( $10 \rightarrow 7$  in MtrF, 1 T-shaped pair) to a  
298 factor of  $\approx 10^3$  ( $10 \rightarrow 5$  in MtrC, 1 co-planar and 2 T-shaped  
299 pairs). Without the Cys-mediated coupling enhancement, the  
300 co-planar or T-shaped heme pairs in the middle of the protein  
301 limit the electron flux, whereas with coupling enhancement  
302 these ET steps become similarly fast as ET between stacked  
303 heme pairs. In this case there is no longer a clearly flux-  
304 limiting ET step; the two slowest steps are within an order of  
305 magnitude.

306 **Discussion.** Although direct experimental estimates for heme-  
307 to-heme ET rate constants in solvated single-molecule MtrC  
308 and MtrF have not (yet) been reported, measurements have  
309 been carried out on related systems that lend support to some  
310 of our results. First, Butt and co-workers investigated the  
311 MtrC containing MtrCAB protein complex inserted in a proteo-  
312 liposome and adsorbed on a Fe(III)-oxide nano-particle(38).  
313 The electron flux from an excess soluble electron donor across  
314 the entire MtrCAB complex on to the oxide was determined  
315 to be  $10^4 \text{ s}^{-1}$ . It was shown that the rate was limited by the  
316 heterogeneous ET step from the protein to the oxide, hence  
317 should be considered a lower bound to the protein-limited rate.  
318 Our estimate for the latter,  $10^5 \text{ s}^{-1}$ , is thus in line with this  
319 experimental result.

320 Second, El-Naggar and co-workers recently reported electro-  
321 chemical gating experiments on *Shewanella oneidensis* MR1  
322 cells(39), which require the Mtr pathway cytochromes (in  
323 particular MtrC) for electron transfer to the electrodes. Mea-  
324 suring the conduction current as a function of temperature,  
325 Arrhenius behaviour was observed and the thermal activa-  
326 tion energy for electron transport determined to be 0.29 eV.  
327 This compares very favourably with the calculated largest  
328 activation free energy for heme-to-heme hopping steps along  
329 the octa-heme chain,  $\Delta A^\ddagger = (\lambda + \Delta A)^2 / (4\lambda) = 0.33 \text{ eV}$  in the  
330  $10 \rightarrow 5$  direction (heme pair 6-1), and  $\Delta A^\ddagger = 0.29 \text{ eV}$  in the  
331  $10 \leftarrow 5$  direction (heme pair 8-6).

332 A third type of experiment one could compare our re-  
333 sults to are the  $I-V$  measurements by Rosso, El-Naggar and  
334 co-workers on single MtrC(9) and MtrF(11) proteins using  
335 STM. Assuming the same hopping mechanism as for ET in  
336 solution(11, 28, 40, 41), we obtain currents of a few 0.1 nA  
337 at 0.5 V bias voltage for MtrC and MtrF, respectively, in  
338 good agreement with experiments(9, 11) (see SI Appendix,  
339 fig. S2). By contrast, without the Cys-mediated electronic  
340 coupling enhancement, the currents are two orders of mag-  
341 nitude too low. The favourable comparison with the STM  
342 currents should be considered with some caution, however,  
343 since a number of assumptions went into the modelling (see  
344 SI Appendix for discussion.) In this regard, we note that  
345 recent  $I-V$  measurements on MtrF monolayer junctions  
346 reported temperature-independent transport, which is incom-  
347 patible with thermally activated hopping(12). However, the

348 experimental conditions in this latter study are quite differ-  
349 ent with respect to the above mentioned STM measurements  
350 (high-vacuum vs air, protein monolayer vs single molecule, sus-  
351 pended nanowire vs tip) which may tip the balance between  
352 different mechanisms.

353 Finally, we wish to investigate whether the popular path-  
354 way model(33, 34) can capture the rate enhancements due  
355 to the heme side chains as predicted by present DFT/POD  
356 calculations. To this end we have calculated the enhancement  
357 factor  $r_{\text{pw}} = \langle |H_{\text{ab}}^{\text{pw}}|^2 \rangle / \langle |H_{\text{ab}}^{\text{ts}}|^2 \rangle$ , where  $H_{\text{ab}}^{\text{pw}}$  and  $H_{\text{ab}}^{\text{ts}}$   
358 are the pathway (pw) coupling matrix elements for heme-to-heme elec-  
359 tron tunneling along the strongest coupling path in the large  
360 QM model (typically through-space via side chains) and in  
361 the minimum QM model (through-space edge to edge), and  
362  $\langle \dots \rangle$  denotes the thermal average over MD snapshots. In the  
363 following we compare  $r_{\text{pw}}$  with  $r_{\text{dft}}$  defined in section *Results*.  
364 We find values  $r_{\text{pw}} = 2200$  ( $r_{\text{dft}} = 2500$ ) for the co-planar heme  
365 pair 1-6 and 120 (38) and 170 (11) for the T-shaped heme  
366 pairs 8-6 and 1-3 for pathway (DFT/POD) calculations on  
367 MtrC, and similar results for MtrF (see SI Appendix, Table  
368 S3). The agreement is excellent for the heme pair 1-6 that  
369 limits the overall electron flow and semi-quantitative overall.  
370 Yet, the pathway model incorrectly predicts rate enhancements  
371 of the same size if the S atom of the Cys linkages is changed  
372 into  $\text{CH}_2$ (32). This problem could be addressed by including  
373 chemical specificity in a refined version of the pathway model.

374 **Concluding Remarks.** We found that both MtrC and MtrF  
375 form a tri-furcated electron conduit that channels electrons  
376 with similar efficiency in perpendicular ( $10 \leftrightarrow 5$ ) and parallel  
377 ( $7 \leftrightarrow 2$ ) directions relative to the outer-membrane. The elec-  
378 tron flow is reversible implying that both proteins not only  
379 support electron export but also electron import, a feature that  
380 enables electrode-driven electrosynthesis of chemicals inside  
381 the bacterial cell(5-8, 42). The tri-furcation of the electron  
382 flow in MtrC and MtrF is achieved by two junctions in the  
383 middle of the protein comprised of heme pairs with relatively  
384 large edge-to-edge tunneling distances (T-shaped, co-planar).  
385 Intriguingly, our calculations indicate that the junctions do  
386 not slow down the electron flux because Cys linkages inserting  
387 in the space between these heme pairs significantly enhance  
388 electronic coupling by reducing the effective tunneling distance.  
389 The same effect has been observed before for the two T-shaped  
390 pairs in the smaller tetra-heme cytochrome STC(32) implying  
391 that the coupling enhancement could be an evolutionary de-  
392 sign principle of significance to the entire class of multi-heme  
393 cytochromes.

394 We note that there is little difference in the protein-limited  
395 electron flow through MtrC and MtrF. While reorganization  
396 free energies are slightly lower in MtrC than in MtrF, in line  
397 with reduced solvent accessible surface area of its hemes, no  
398 significant differences in electronic coupling are discernable.  
399 Thus, from the perspective of redox function our characteriza-  
400 tion suggests that MtrC can be replaced by MtrF, as in fact  
401 observed experimentally.(29, 30) The higher expression levels  
402 of MtrCAB relative to MtrFDE at low  $\text{O}_2$  concentrations(43)  
403 is thus more likely related to a genetic origin rather than  
404 electron transfer function.

405 Efficient ET in MtrC in the direction parallel to the outer-  
406 membrane is one of the prerequisites for micrometer-long  
407 electronic conduction along cellular appendages as observed in  
408 Ref.(22) Whether the intraprotein ET in MtrC studied here or

the interprotein ET between adjacent MtrCAB complexes is the flux-limiting process remains to be investigated. According to the cryomicroscopy study of Ref. (19) adjacent MtrCAB complexes may be separated by more than 30 nm, as depicted in fig. 1E. Hence, the answer to this question will depend on the diffusivity of the MtrCAB protein complex in the outer membrane and the kinetics of the interprotein ET step between two interacting MtrC proteins. Modelling of these processes will require a suitable representation of MtrCAB, possibly coarse-grained to study its diffusivity on long time scales, as well as an atomistic structure of the MtrC-MtrC interface.

## Materials and Methods

Molecular dynamics simulations were carried for aqueous MtrC and NrfB at room temperature starting from the crystal structures pdb id 1M1Q(44) and pdb id 2OZY(13), respectively, using the AMBER03 force field(45) and the TIP3P water model(46). Driving forces ( $\Delta A_{ji}$ ) for MtrC and reorganization free energies ( $\lambda$ ) for MtrC and NrfB were obtained from MD stimulation as described for MtrF(26, 35). Heme-heme electronic coupling matrix elements ( $H_{ab}$ ) were calculated for MtrC and MtrF as described in Ref. (32) using the projection operator-based diabaticization (POD) method(47, 48) in combination with a modified PBE functional where 50% GGA exchange is replaced by Hartree-Fock exchange. This method showed excellent performance(48) against high-level ab initio reference values on dimers of the HAB11 database.(49). Full computational details can be found in the SI Appendix.

**ACKNOWLEDGMENTS.** X.J. was supported by a Ph.D. studentship co-sponsored by the Chinese Scholarship Council and University College London. Z.F. was supported by EPSRC Grant No. EP/M001946/1. J.B. was supported by the European Research Council (ERC) under the European Unions Horizon 2020 research and innovation programme (grant agreement no. 682539/SOFTCHARGE). Via our membership of the UKs HEC Materials Chemistry Consortium, which is funded by EPSRC (EP/L000202), this work used the ARCHER UK National Supercomputing Service (<http://www.archer.ac.uk>). The authors acknowledge the use of the UCL Legion High Performance Facility (Legion@UCL).

1. Myers CR, Nealon KH (1988) Bacterial manganese reduction and growth with manganese oxide as the sole electron acceptor. *Science* 240:1319–1321.
2. Zhuang K, Ma E, Lovley DR, Mahadevan R (2012) The design of long-term effective uranium bioremediation strategy using a community metabolic model. *Biotechnol Bioeng.* 109:2475–2483.
3. Yi H, et al. (2009) Selection of a variant of geobacter sulfurreducens with enhanced capacity for current production in microbial fuel cells. *Biosens. Bioelect.* 24:3498–3503.
4. Fitzgerald LA, et al. (2012) Aggrandizing power output from shewanella oneidensis mr-1 microbial fuel cells using calcium chloride. *Biosens. Bioelect.* 31:492–498.
5. Ross DE, Flynn JM, Baron DB, Gralnick JA, Bond DR (2011) Towards electrosynthesis in shewanella: energetics of reversing the mtr pathway for reductive metabolism. *PLoS ONE* 6:e16649.
6. Lovley DR (2012) Electromicrobiology. *Annu. Rev. Microbiol.* 66:391–409.
7. Schroder U, Harnisch F, Angenent LT (2015) Microbial electrochemistry and technology: terminology and classification. *Energy Environ. Sci.* 8:513–519.
8. Chong GW, Karbelkar AA, El-Naggar MY (2018) Nature's conductors: what can microbial multi-heme cytochromes teach us about electron transport and biological energy conversion? *Curr. Opin. Chem. Biol.* 47:7–17.
9. Wigginton NS, Rosso KM, Lower BH, Shi L, Hochella MFJ (2007) Electron tunneling properties of outer-membrane decaheme cytochromes from shewanella oneidensis. *Geochim. Cosmochim. Acta* 71:543–555.
10. Leung KM, et al. (2013) Shewanella oneidensis mr-1 bacterial nanowires exhibit p-type, tunable electronic behavior. *ACS Nano* 13:2407–2411.
11. Byun HS, Pirbadian S, Nakano A, Shi L, El-Naggar MY (2014) Kinetic monte carlo simulations and molecular conductance measurements of the bacterial decaheme cytochrome mtrF. *ChemElectroChem* 1:1932–1939.
12. Garg K, et al. (2018) Direct evidence for heme-assisted solid-state electronic conduction in multi-heme c-type cytochromes. *Chem. Sci.* 9:7304–7310.
13. Clarke TA, Cole JA, Richardson DJ, Hemmings AM (2007) The crystal structure of the penta-haem c-type cytochrome nrfb and characterization of its solution-state interaction with the penta-haem nitrite reductase nrfA. *Biochem. J.* 406:19.

14. Paixao VB, et al. (2008) The solution structure of a tetraheme cytochrome from shewanella frigidimarina reveals a novel family structural motif. *Biochemistry* 47:11973–11980.
15. Clarke TA, et al. (2011) et al. structure of a bacterial cell surface decaheme electron conduit. *Proc. Natl. Acad. Sci. USA* 108:9384–9389.
16. Edwards MJ, et al. (2012) The crystal structure of the extracellular 11-heme cytochrome unda reveals a conserved 10-heme motif and defined binding site for soluble iron chelates. *Structure* 20:1275–1284.
17. Edwards MJ, et al. (2015) et al. redox linked flavin sites in extracellular decaheme proteins involved in microbe-mineral electron transfer. *Sci. Rep.* 5:11677.
18. Pirbadian S, et al. (2014) Shewanella oneidensis mr-1 nanowires are outer membrane and periplasmic extensions of the extracellular electron transport components. *Proc. Natl. Acad. Sci.* 111:12883–12888.
19. Subramanian P, Pirbadian S, El-Naggar MY, Jensen GJ (2018) Ultrastructure of shewanella oneidensis mr-1 nanowires revealed by electron cryotomography. *Proc. Nat. Acad. Sci. USA* 115:E3246–E3255.
20. Vargas M, et al. (2013) Aromatic amino acids required for pili conductivity and long-range extracellular electron transport in geobacter sulfurreducens. *mBio* 4(2):e00210–13.
21. Adhikari RY, Malvankar NS, Tuominen MT, Lovley DR (2016) Conductivity of individual geobacter pili. *RSC Adv.* 6:8354–8357.
22. El-Naggar MY, et al. (2010) Electrical transport along bacterial nanowires from shewanella oneidensis mr-1. *Proc. Natl. Acad. Sci. USA* 107:18127–18131.
23. Blumberger J (2018) Electron transfer and transport through multi-heme proteins: recent progress and future directions. *Curr. Opin. Chem. Biol.* 47:24–31.
24. Breuer M, Rosso KM, Blumberger J, Butt JN (2015) Multi-heme cytochromes in shewanella oneidensis mr-1: Structures, functions and opportunities. *J. R. Soc. Interface* 12:20141117.
25. Blumberger J (2015) Recent advances in the theory and molecular simulation of biological electron transfer reactions. *Chem. Rev.* 115:11191–11238.
26. Breuer M, Zarzycki P, Blumberger J, Rosso KM (2012) Thermodynamics of electron flow in the bacterial deca-heme cytochrome mtrF. *J. Am. Chem. Soc.* 134:9868–9871.
27. A. Barrozo, M. Y. El-Naggar AIK (2018) Distinct electron conductance regimes in bacterial decaheme cytochromes. *Angew. Chem. Int. Ed.* 57:6805–6809.
28. Breuer M, Rosso KM, Blumberger J (2014) Electron flow in multi-heme bacterial cytochromes is a balancing act between heme electronic interaction and redox potentials. *Proc. Nat. Acad. Sci. USA* 111:611–616.
29. Bucking C, Popp F, Kerzenmacher S, Gescher J (2010) Involvement and specificity of shewanella oneidensis outer membrane cytochromes in the reduction of soluble and solid-phase terminal electron acceptors. *FEMS Microbiol. Lett.* 306:144–151.
30. Coursolle D, Gralnick JA (2012) Reconstruction of extracellular respiratory pathways for iron(III) reduction in shewanella oneidensis strain mr-1. *Front. Microbiol.* 3:56.
31. Leys D, et al. (2002) Crystal structures at atomic resolution reveal the novel concept of  $\mu$ -electron-harvesting  $\text{Fe}^{\text{II}}$  as a role for the small tetraheme cytochrome c. *J. Biol. Chem.* 277:35703–35711.
32. Jiang X, et al. (2017) Cysteine linkages accelerate electron flow through tetra-heme protein stc. *J. Am. Chem. Soc.* 139:17237–17240.
33. Beratan DN, Onuchic JN, Hopfield JJ (1987) Electron tunneling through covalent and noncovalent pathways in proteins. *J. Chem. Phys.* 86:4488–4498.
34. Beratan DN, et al. (2015) Charge transfer in dynamical biosystems, or the treachery of (static) images. *Acc. Chem. Res.* 48:474–481.
35. Breuer M, et al. (2012) Molecular structure and free energy landscape for electron transport in the deca-heme cytochrome mtrF. *Biochem. Soc. Trans.* 40:1198–1203.
36. Winn MD, et al. (2011) Overview of the ccp4 suite and current developments. *Acta Cryst. Sec. D* 67:235.
37. Blumberger J (2008) Free energies for biological electron transfer from qm/mm calculation: method, application and critical assessment. *Phys. Chem. Chem. Phys.* 10:5651–5667.
38. White GF, et al. (2013) Rapid electron exchange between surface-exposed bacterial cytochromes and Fe(III) minerals. *Proc. Nat. Acad. Sci. USA* 110:6346–6351.
39. Xu S, Barrozo A, Tender LM, Krylov AI, El-Naggar MY (2018) Multiheme cytochrome mediated redox conduction through shewanella oneidensis mr-1 cells. *J. Am. Chem. Soc.* 140:10085–10089.
40. Polizzi NF, Skourtis SS, Beratan DN (2012) Physical constraints on charge transport through bacterial nanowires. *Faraday Discuss.* 155:43–62.
41. Pirbadian S, El-Naggar MY (2012) Multistep hopping and extracellular charge transfer in microbial redox chains. *Phys. Chem. Chem. Phys.* 14:13802.
42. Rabaey K, Rozendal RA (2010) Microbial electrosynthesis - revisiting the electrical route for microbial production. *Nat. Rev. Microbiol.* 8:706–716.
43. Barchinger SE, et al. (2016) Regulation of gene expression in shewanella oneidensis mr-1 during electron acceptor limitation and bacterial nanowire formation. *Appl. Environ. Microbiol.* 82:5428–5443.
44. Edwards MJ, et al. (2015) Redox linked flavin sites in extracellular decaheme proteins involved in microbe-mineral electron transfer. *Sci. Rep.* 5:11677.
45. Duan Y, et al. (2003) A point-charge force field for molecular mechanics simulations of proteins based on condensed-phase quantum mechanical calculations. *J. Comp. Chem.* 24:1999.
46. Jorgensen WL, Chandrasekhar J, Madura JD, Impey RW, Klein ML (1983) Comparison of simple potential functions for simulating liquid water. *J. Chem. Phys.* 79:926–935.
47. Kondov I, Cizek M, Benesch C, Wang H, Thoss M (2007) Quantum dynamics of photoinduced electron-transfer reactions in dye-semiconductor systems: A first-principles description and application to coumarin 343-tio2. *J. Phys. Chem. C* 111:11970–11981.
48. Futera Z, Blumberger J (2017) Electronic couplings for charge transfer across molecule/metal and molecule/semiconductor interfaces: performance of the projector operator-based diabaticization approach. *J. Phys. Chem. C* 121:19677–19689.
49. Kubas A, et al. (2014) Electronic couplings for molecular charge transfer: benchmarking cdf, fodft and fodftb against high-level ab initio calculations. *J. Chem. Phys.* 140:104105–21.